

History Dependence in a Chemical Reaction Network Enables Dynamic Switching

Dmitrii V. Kriukov, A. Hazal Koyuncu, and Albert S. Y. Wong*

This work describes an enzymatic autocatalytic network capable of dynamic switching under out-of-equilibrium conditions. The network, wherein a molecular fuel (trypsinogen) and an inhibitor (soybean trypsin inhibitor) compete for a catalyst (trypsin), is kept from reaching equilibria using a continuous flow stirred tank reactor. A so-called ‘linear inhibition sweep’ is developed (i.e., a molecular analogue of linear sweep voltammetry) to intentionally perturb the competition between autocatalysis and inhibition, and used to demonstrate that a simple molecular system, comprising only three components, is already capable of a variety of essential neuromorphic behaviors (hysteresis, synchronization, resonance, and adaptation). This research provides the first steps in the development of a strategy that uses the principles in systems chemistry to transform chemical reaction networks into platforms capable of neural network computing.

1. Introduction

Recent progress in artificial neural networks shows that computers can perform intelligent tasks (and in some cases outperform the human brain).^[1] Artificial intelligence, however, requires enormous amounts of energy and new types of hardware, with different energy requirements as compared to conventional silicon-based components, are urgently needed.^[2] Material capable of basic features of learning and adaptation, particularly, would allow novel concepts in artificial intelligence and may complement current efforts in neuromorphic com-

puting.^[3] Advances in the design of molecular circuits based on deoxyribonucleic acid (DNA),^[4,5] Belousov–Zhabotinsky reactions, BZ,^[6] and molecular thin-films^[7,8] demonstrate that a molecular-level decisions could provide in-memory computing capabilities. These examples incorporate elements of systems biology, excitable periodic functions, and control theory, respectively, to derive molecular-based learning circuits. To pave a way that evades from implementations reminiscent of logic gates in traditional computing, however, we need new design strategies that can go beyond Nature’s most versatile macromolecule (DNA),^[9] chemistry’s most well-known oscillating system (BZ),^[10] or one of nanotechnology’s most used fabrication method.^[11]


We believe that chemical reaction networks (CRNs) may provide a novel molecular hardware. The discovery of network motifs and feedback loops^[12,13] in biochemical, metabolic, or genetically regulated networks^[14]—widely accepted as the basic building blocks of complex systems^[15]—sparked enormous activity in systems chemistry.^[16] The theoretical framework for CRNs is well-established^[17–19] and the experimental framework is gaining ground rapidly, with examples demonstrating that small sets of chemical reactions can already construct systems with complex behavior such as bistability,^[20] oscillations,^[21] and transient assemblies.^[22,23] The common challenge many of these efforts face, however, is that the underlying design remains relatively simple, limited to a set of network motifs, and strategies to rationally expand complexity in a modular way are scarce. Hence, rationalizing the ability to learn, and the capacity to adapt to an environment, exceeds current synthetic designs.^[24]

Here, we use a systems chemistry approach to develop a novel method to control the systems’ dynamics. By examining how such CRNs can respond to changes in gradients, we demonstrate that an out-of-equilibrium CRN is capable of history-dependent functions such as hysteresis, resonance, and adaptation (i.e., essential components for neuromorphic computing^[25,26]). Our work builds on our previously reported autocatalytic network.^[27] Briefly, our network comprises a positive feedback loop and an inhibitor which can suppress activation of the positive feedback. Autocatalytic reactions are essentially bistable (they exhibit two stable steady-state outputs for one input value^[28]) and can provide a nonlinear activation step when maintained under flow conditions (using a continuous flow stirred tank reactor, CSTFR^[29]). We depict the process in **Figure 1a**: The inhibitor (*I*) first reacts with trypsin (*Tr*) and delays the reaction of *Tr* with trypsinogen (*Tg*). When all inhibitor has reacted, *Tg* either

D. V. Kriukov, A. H. Koyuncu, A. S. Y. Wong
Department of Molecules and Materials
Faculty of Science and Technology
University of Twente
Drienerlolaan 5, Enschede 7522 NH, The Netherlands
E-mail: albert.wong@utwente.nl

A. S. Y. Wong
MESA+ Institute for Nanotechnology
University of Twente
Drienerlolaan 5, Enschede 7522 NH, The Netherlands

A. S. Y. Wong
BRAINS (Center for Brain-inspired Nano Systems)
University of Twente
Drienerlolaan 5, Enschede 7522 NH, The Netherlands

 The ORCID identification number(s) for the author(s) of this article can be found under <https://doi.org/10.1002/smll.202107523>.

© 2022 The Authors. Small published by Wiley-VCH GmbH. This is an open access article under the terms of the Creative Commons Attribution License, which permits use, distribution and reproduction in any medium, provided the original work is properly cited.

DOI: 10.1002/smll.202107523

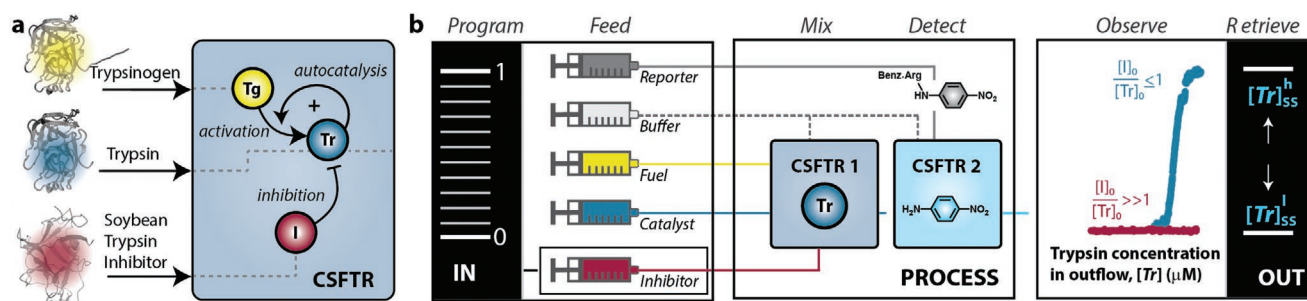


Figure 1. Information processing using a simple autocatalytic reaction network. a) Illustration of a continuous flow stirred tank reactor (CFSTR), that was used to control the in- and outflow of enzymes trypsin (Tr), trypsinogen (Tg), and soybean trypsin inhibitor (I). Autocatalytic network consists of three main reactions: activation, autocatalysis, inhibition. Details of their mechanisms are provided in Section S4.1, Supporting Information. b) Schematic representation of the experimental platform (details are provided in Section S3, Supporting Information). The network in a produces two different steady states (which we measured by the activity of trypsin, see Section 4): A high steady state ($[Tr]_{ss}^h$), and a low steady state ($[Tr]_{ss}^l$).

auto-activates, or Tr catalyzes, the conversion of Tg into Tr to yield an autocatalytic production of Tr .

Inspired by how a living cell processes information^[30,31]—which can dynamically regulate effective concentrations of chemical components in a biological pathways^[32]—we exploited the possibilities of modulating the response of our network using the inhibitor concentration as an input signal (Figure 1b). To ensure that the inhibitor acts as an initial suppressor in this network (and not as a delayed inhibition step), we used soybean trypsin inhibitor as it is a protein that can bind Tr fast and irreversibly^[33] (Figures S1 and S2, Supporting Information). We programmed the input signal to perturb the autocatalytic network, and found that the response of the system critically depended on its preceding state. We demonstrate that this simple bistable system can exhibit history-dependent properties in both its steady and its transient states.

2. Results and Discussion

2.1. Bistability Obtained in Flow Conditions

The continuous supply of reactants was achieved using independent syringe pumps for each component (Figure 1b). In this experimental setup, Tg acts as a fuel for generating the catalyst Tr and its process is regulated by the inhibitor concentration ($[I]_o$). Other syringes (containing the buffer and $N\alpha$ -Benzoyl-DL-arginine 4-nitroanilide hydrochloride, BAPNA) were used to control the pH and to enable the readout of the Tr activity in the outflow (which we used to characterize the steady state of the network). Ultimately, the concentration of Tr stabilizes as the inflow of new reactants is balanced with the outflow of Tr and (unreacted) Tg and I . This system has reached one of its two outputs ($[Tr]_{ss}$): The low steady state ($[Tr]_{ss}^l$, red signal) is reached when the catalyst is the limiting reactant ($[I]_o/[Tr]_o \gg 1$). In all other cases ($[I]_o/[Tr]_o \leq 1$), a high steady state ($[Tr]_{ss}^h$, cyan signal) is reached.

2.2. History Dependency in a Bistable Network

Using this setup, we programmed input sequences to probe the history dependence in our system. As depicted in

Figure 2a, we first used a continuous inflow of $[I]_{-1} = 10 \mu\text{M}$ that allowed the system to reach a low $[Tr]_{-1}$ ($4.0 \pm 0.2 \mu\text{M}$). Subsequently, we changed the $[I]_o$ to a value between 0.5 and 10 μM in separate experiments. For instance, when $[I]_o$ was changed to 3 μM , we found that the system established a $[Tr]_{ss}([I]_{-1}; [I]_o) = 70.7 \pm 1.2 \mu\text{M}$. A similar procedure was applied to examine the steady states with the same input values for $[I]_o$, but with a high $[Tr]_{-1}$ ($74.5 \pm 1.9 \mu\text{M}$) as the preceding state (Figure 2b). This clearly demonstrates that even high concentrations of inhibitor are not sufficient to significantly suppress the $[Tr]_{ss}$ after high concentrations of Tr have accumulated in the CFSTR in the preceding state. These results, thus, show that the steady state of the network either *i*) changes abruptly around a critical value between $[I]_o = 5\text{--}8 \mu\text{M}$ when $[Tr]_{ss}^l$ was reached in the preceding state, or *ii*) remains unchanged when $[Tr]_{ss}^h$ was reached in the preceding state (Figure 2c), and can be summarized this observation as follows:

$$\text{If } [I]_{-1} = 10 \mu\text{M} : [Tr]_{ss}(10, [I]_o) = \begin{cases} [Tr]_{ss}^h, & \text{when } [I]_o < 5.0 \\ [Tr]_{ss}^l, & \text{when } [I]_o > 8.0 \end{cases} \quad (1)$$

$$\text{If } [I]_{-1} = 0.5 \mu\text{M} : [Tr]_{ss}(0.5, [I]_o) = [Tr]_{ss}^h \quad (2)$$

These trends are in excellent agreement with the thermodynamic and kinetic branches (steady state solutions that are characteristic to autocatalytic reactions under flow conditions^[29]), which we simulated based on the set of ordinary differential equation (see Section S4, Supporting Information).

Using our mathematical model, we projected the difference in the steady states ΔTr (i.e., $[Tr]_{ss}(0.5, [I]_o)$ was subtracted from $[Tr]_{ss}(10, [I]_o)$) at a range of flow rates and inhibitor concentrations in a so-called phase plot (Figure 2d). The phase plot (or heat map) depicts the conditions wherein the steady state of the system is determined by a preceding state (colored area). This region is, thus, history dependent. Outside of this region, the system shows no history dependency either because *i*) high inhibitor concentrations and high flow rates combined outcompete the rate of Tg activation (Phase I), or *ii*) inhibitor concentrations are too low to play a significant role in controlling Tr autocatalysis (Phase II). Overall, the phase plot demonstrates that the characteristic nonlinear response (i.e., the sharp transition around $[I]_o = 5 \mu\text{M}$ observed in our experiments,

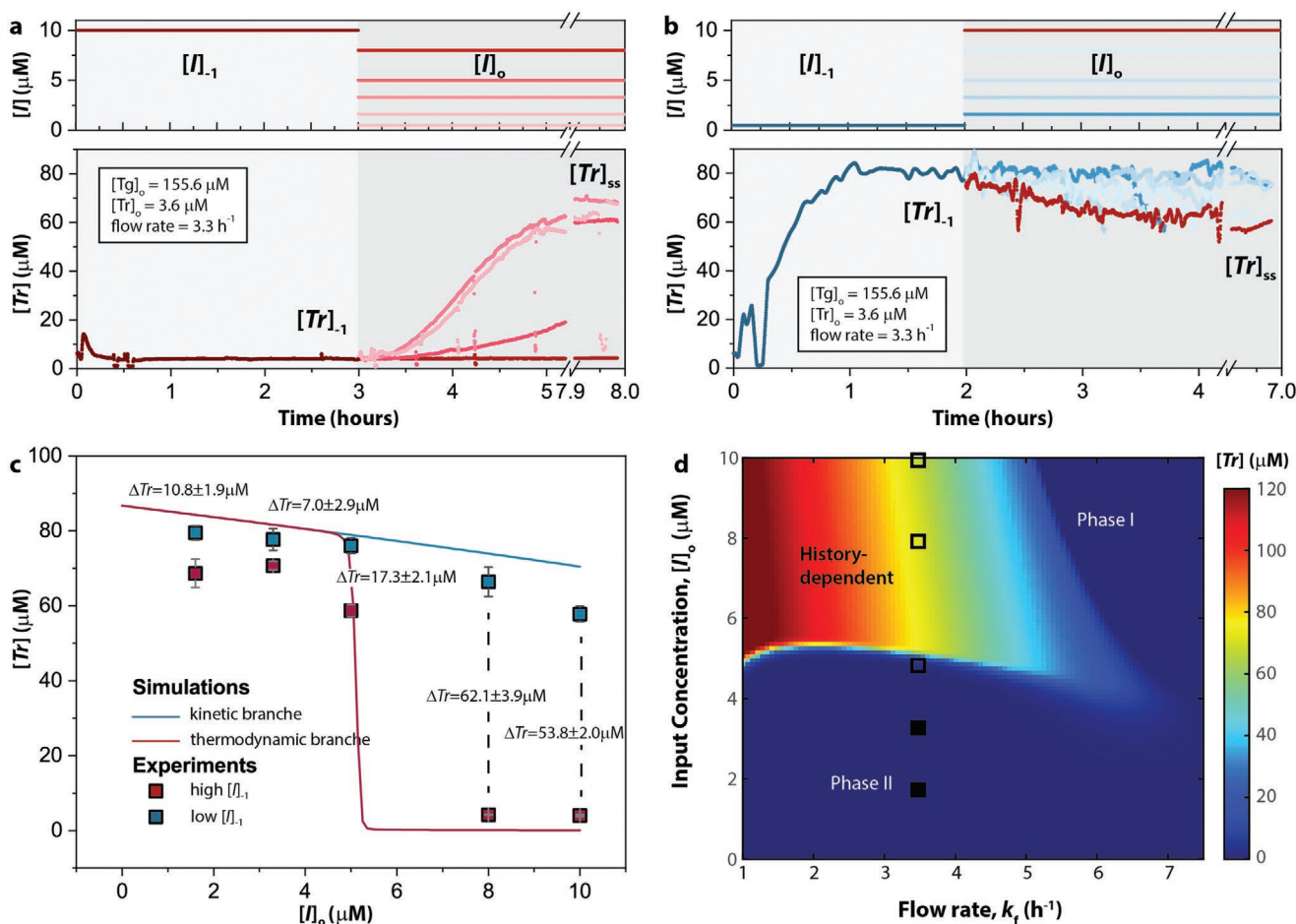


Figure 2. History-dependent states created by stable and transient states. Time traces showing the response of the network when input $[I]_{-1}$ was changed to $[I]_0$, a) from a high to low(er) $[I]_0$, and b) from a low to high(er) $[I]_0$. $[Tr]_{-1}$ indicates the preceding steady state, and $[Tr]_{ss}$ indicates the subsequent steady state. Initial conditions are indicated in the legend. Other conditions are: $\text{pH} = 7.8$, and $T = \text{room temperature}$. c) Experimentally determined steady states of the network, $[Tr]_{ss}$, as a function of the inhibitor concentration, $[I]_0$. Similar trends were obtained by simulations (for details, see Section S4, Supporting Information). The differences between states of the respective branches, $\Delta[Tr]_{ss}$, was determined by subtracting the experimental data set highlighted in red from the set highlighted in blue. d) Phase plot showing the $\Delta[Tr]$ as a result of a history-dependent process (for details see Section 4). Initial conditions for simulations were identical to the experimental data set (indicated with closed squares for low $[Tr]_{ss}$, open squares for high $[Tr]_{ss}$).

black squares) can be obtained at various flow rates. Notably, the history-dependent region is completely different when we compared the steady states at a range of flow rates and trypsin concentrations (Figure S10, Supporting Information). This phase plot, in contrast to Figure 2d, wherein nonlinearity weakens at greater flow rates, shows that the boundary critically depends on the flow rate k_f (and not on the input concentration, in accordance with our observation in Figure 2b).

2.3. Hysteresis, Resonance, and Adaptation Obtained in Linear Inhibition Sweep-Conditions

The use of transient rather than steady states can extend the history-dependent region (Figure S11, Supporting Information). Furthermore, it allows for dynamic input functions that are frequently applied in studies on resistive switching mechanisms.^[34] An example of such dynamic input is a 'linear inhibition

sweep' (LIS) (i.e., we use a molecular analogue of linear sweep voltammetry). Figure 3a shows a simulation with a sweep rate that was 50 times smaller than the applied flow rate (i.e., $k_f/k_s = 50$). The system essentially approaches a steady state in each step and under these conditions $[Tr]$ first increases near the end of the negative gradient and decreases almost immediately when the positive gradient was initiated. That the opposed reactions follow a different path can also be seen in the insert: The network autocatalyzes with a maximum rate at $[I] \approx 2 \mu\text{M}$, while it inhibits with a maximum rate around at $[I] \approx 6 \mu\text{M}$. When we increased the sweep rate tenfold (i.e., $k_f/k_s = 5$), however, this characteristic shape was amplified and shifted (Figure 3b, insert). The autocatalytic production of Tr was activated to close to $[I] \approx 0.5 \mu\text{M}$ (the point after which the inhibitor concentration increased) and could therefore not generate a sufficient level of Tr before the inhibition started to outcompete autocatalysis. Accordingly, we observed a displacement of the local maximum and a time-trace that was surprisingly symmetric.

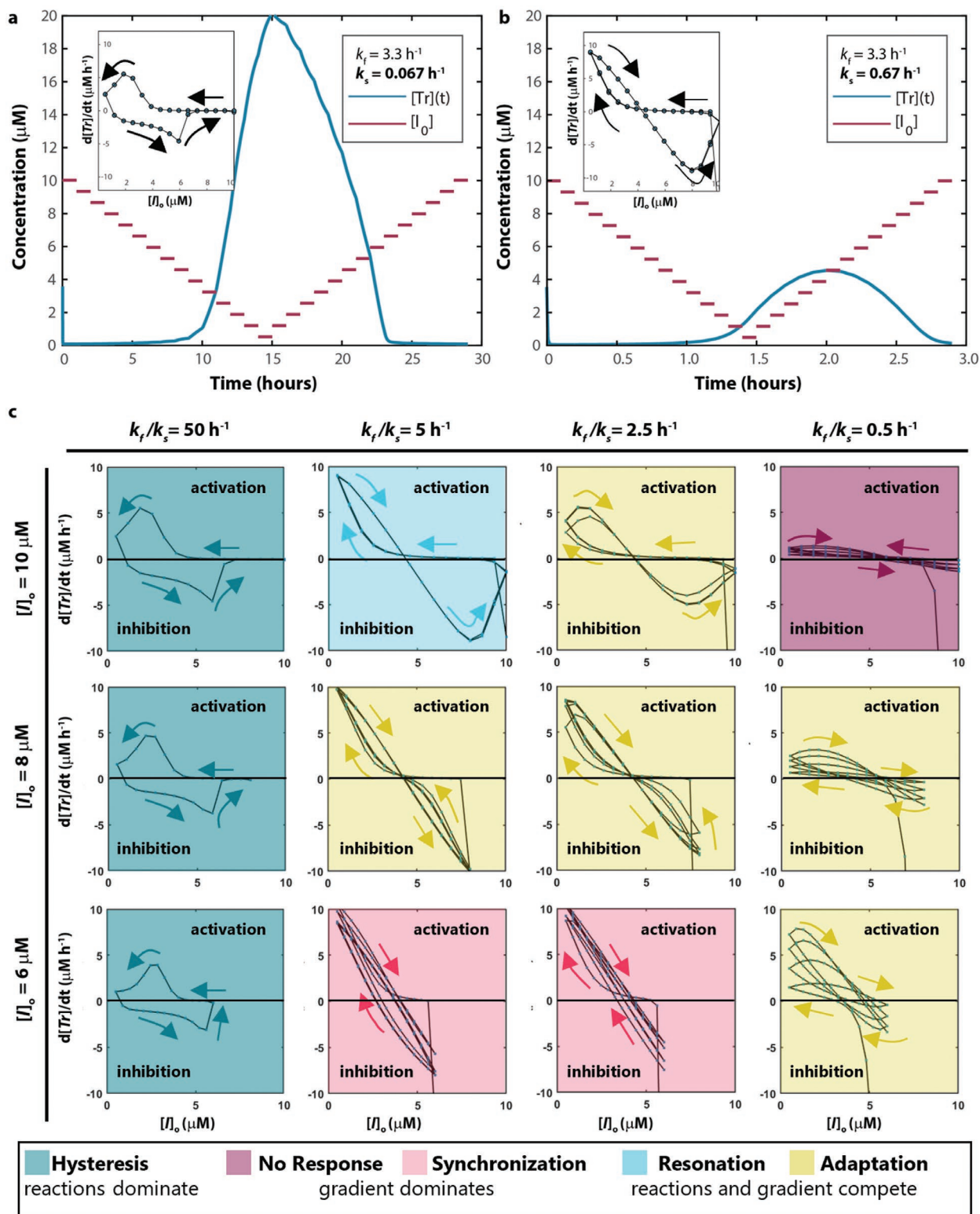


Figure 3. Simulated response of the autocatalytic network to linear inhibition sweeps. Time series of Tr with an input inhibitor concentration that was changed using a negative gradient (comprising 15 steps) to switch from $[I]_{-1} = 10 \mu\text{M}$ to $[I]_o = 0.5 \mu\text{M}$ and a positive gradient to return to $[I]_o$. The sweep rate was achieved in a) 1 h per step, resulting in a flow rate/sweep rate, $k_f/k_s = 50 \text{ h}^{-1}$, and b) 0.1 h per step, resulting in a $k_f/k_s = 5 \text{ h}^{-1}$. c) Phase portraits of the network under repetitive linear inhibition sweeps. The derivative, $d\text{Tr}/dt$, of time series (see Figures S12–S14, Supporting Information) depict the rate of the reaction trajectory. Positive values indicate that the reaction is in activation, while negative values indicate that the reaction is in inhibition. Characteristic behaviors, varying from a stable hysteric regime (i.e., $k_f/k_s \gg 1$) to an apparent dynamic regime (i.e., when $k_f/k_s < 2.5$ and $[I]_o < 8 \mu\text{M}$), are indicated by colors (see legend). Arrows indicate the direction of the change in the reaction trajectory.

Simulations using various sweeping rates and inhibitor concentrations show that the bistable network can, in principle, provide different classes of behaviors (Figure 3c). In the absence of a sufficient sweep rate ($k_f/k_s \gg 1$, highlighted in cyan), the behavior of the network is fully dependent on the competition between the nonlinear autocatalytic step (i.e., the reaction rate is second order in Tr) and the linear inhibition and depletion steps (both rates are first order in Tr) (for details, see Section S4.1, Supporting Information). As a result, the inhibition route is determined by a different trajectory and reaches a maximum slower than the activation route and a hysteric behavior can be observed (as in Figure 3a). Oppositely, the behavior of the network can become fully dependent on the amplitude and the frequency in the inhibition sweep. The system shows *i*) no response (highlighted in purple), or *ii*) a synchronous response (highlighted in pink).

Under conditions where the reactions, flow and sweep rates compete, more complex behavior such as resonance—the system is able to increase the amplitude when the frequency of a periodically applied force is equal or close to the systems' natural frequency^[35]—and adaptation—the systems is able to adjust to environmental conditions^[36]—may arise. An example of resonance was discussed in Figure 3b and is highlighted in blue. In all other simulated conditions (highlighted in yellow), the trajectory breaks away from an initial response and develops into a synchronous or resonant behavior.

We demonstrate that the network can adjust to changes in the environment and examined the influence of the sweeping rate on the network experimentally. We first used LIS with frequencies smaller than the applied flow rate (Figure 4a,b). Under these conditions, Tr activation occurred before the minimum in the input ($[I]_0$) was reached. When $[I]_{-1} = 8 \mu\text{M}$ was used (Figure 4a), we found that the low Tr concentration could recover after $[I]_{-1}$ was restored. Surprisingly, while the second sweep provided an identical recovery curve as the first sweep, the amplitude in the third sweep was amplified significantly. In another example, when we used $[I]_{-1} = 6 \mu\text{M}$ (Figure 4b), the total inhibitor concentration was not sufficient to allow for a full recovery of the low Tr concentration in the first sweep. Instead, each of the three sequences enabled a new steady state concentration, enabling a continuous build-up of concentrations in Tr until the system settles for a maximum, $[Tr]_{ss}^h$. Hence, these results show that this type of adaptive behavior combines two intrinsic effects of the autocatalytic network: On the one hand, low Tr states are sensitive to perturbations due to the autocatalytic step. On the other hand, high Tr states are robust and therefore difficult to perturb (see Figures S8, Supporting Information, for a validation experiment).

Finally, we increased the sweeping rates from $k_s = 0.67 \text{ h}^{-1}$ to three other values ($k_s = 2.0; 2.7; 4.0 \text{ h}^{-1}$, Figure 4c–e). In these cases, the build-up slowed down significantly because the autocatalytic process could not activate before the minimum in the input ($[I]_0$) was reached in the first sweep. We depict the responses to the LIS's as the rates at which the output $[Tr]$ changes as a function of the $[I]_0$ in Figure 4f–i. These phase portraits show that the direction and magnitude of the reaction is in continuous development, in accordance with the adaptive behavior predicted in Figure 3c. Clearly, the rate of activation and inhibition (or, more precisely, their maxima

either *i*) increase and shift (Figure 4f), *ii*) continuous increase and decrease (Figure 4g), or *iii*) emerge from an initially non-responsive state (highlighted in black) (Figure 4i). We do not yet have a complete theoretical treatment of our observations, but the demonstration that a variety of dynamic behaviors could emerge from a simple autocatalytic network suggests that CRNs may have an inherent resistive nature.

3. Conclusion

This work combines approaches in mathematic modelling and systems chemistry to demonstrate how simple network motifs may provide dynamic and adaptive switching under out-of-equilibrium conditions. We showed how the competition between autocatalysis and inhibition in flow provides the basic parameters for controlling history-dependent functions such as bistability and hysteresis (functions that can be found exclusively when the network is in its steady state). When we used a so-called LIS to probe the history-dependence in the network's transient states, the same motif was capable of more complex behavior such as resonance and adaptation. The LIS, essentially, provided an additional parameter to exploit the nonlinear activation response in autocatalytic networks and to gear CRNs toward novel molecular concepts of adaptive behavior.

We developed a molecular network approach that requires only one simple network motif and used commonly available enzymes and inhibitors to define three basic components of our network (fuel, catalyst, and inhibitor) and easy-to-use CFSTRs to maintain the reactions of these components in flow. The key challenges encountered in the experimental realization of robust steady-state output in CRNs is to balance the reaction rates between various feedback loops in the network^[37] and impede the use of CRNs for information processing purposes. Rather than designing networks of ever greater complexity, we explored the potential of using our autocatalytic network as a single processing unit. We believe that this approach enables novel opportunities to use microliter-sized^[38,39] or multi-coupled^[40] CFSTRs in the experimental mapping of nonlinear activation phenomena with other enzymatic^[41] and autocatalytic reactions.^[42,43] For instance, perturbation experiments applied under repetitive LIS conditions could reveal how CRNs of this type can be switched on and off. These studies can be easily and logically extended to configurations comprising multiple bistable systems in series-, parallel-, or array-coupled CFSTRs to examine how information is transferred between CRNs. Overall, the simple means employed in this research make the design of CRNs amenable to exploit many avenues in the uncharted domain of out-of-equilibrium chemistry, and advance and further enable the design of intelligent materials with potential applications in neuromorphic computing.^[3]

4. Experimental Section

Materials: Bovine trypsinogen (Type I; $\approx 10\,000$ BAEE units mg^{-1}), porcine trypsin (Type II-S, 1000–2000 BAEE units mg^{-1}), N α -Benzoyl-DL-arginine 4-nitroanilide hydrochloride (BAPNA) were purchased

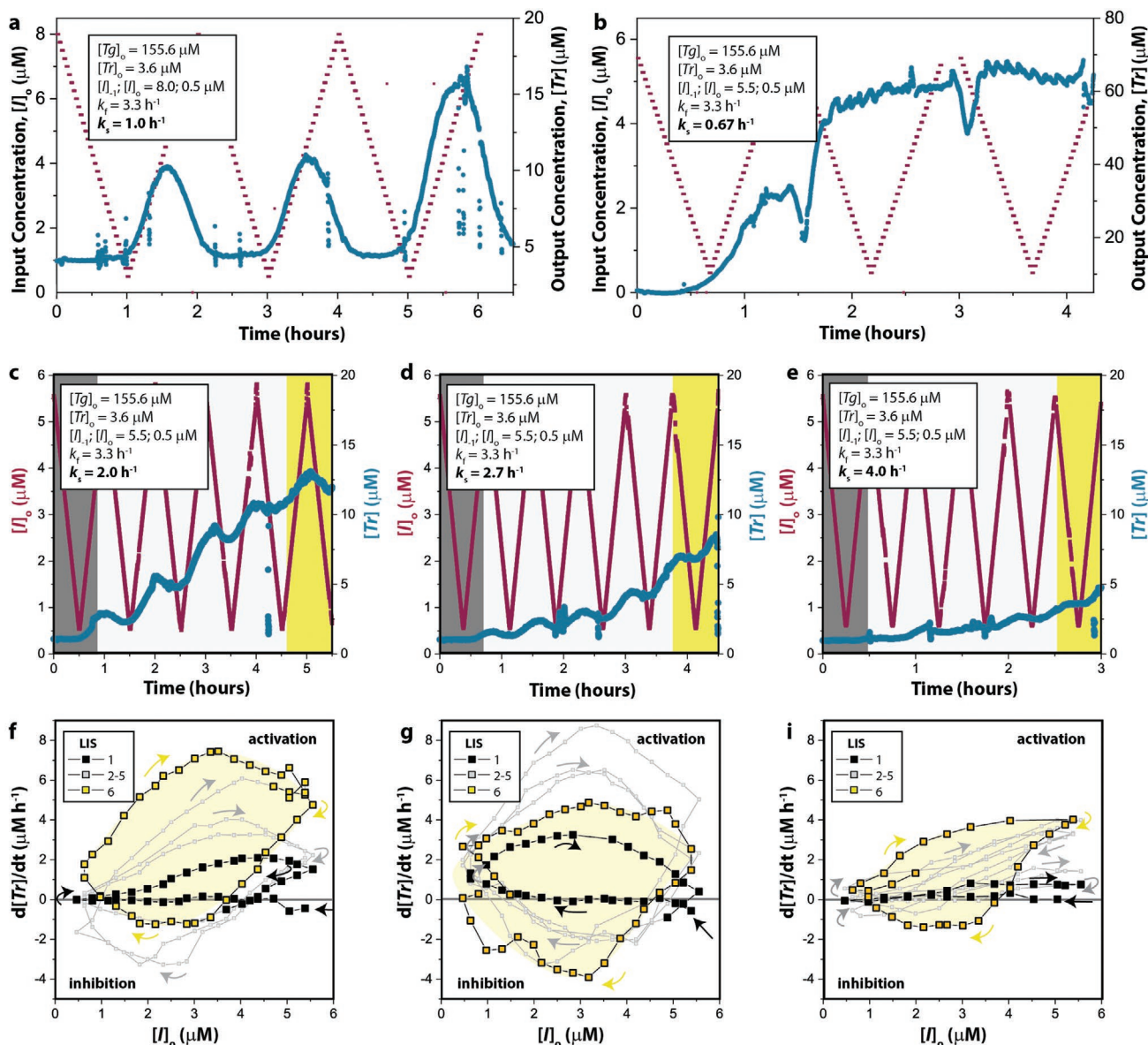


Figure 4. Experimental response of the autocatalytic network to linear inhibition sweeps. a–e) Individual time series of Tr under repetitive linear inhibition sweeps, with initial conditions depicted in the inserts. f–i) Phase portraits of the network under repetitive linear inhibition sweeps. Each datapoint represents the growth/decay in 40 s. Positive values indicate that the reaction is in activation, while negative values indicate that the reaction is in inhibition. The plots are created in origin, after smoothing with a Szavitsky-Golay filter (with point window = 8). Arrows indicate the direction of the reaction trajectory. For (c–i), the colors black, grey, and yellow indicate the outcome in the first, intermediate and final sweep.

from Sigma. Trypsin inhibitor from soybean (STI) was purchased from Roche. Polydimethylsiloxane (PDMS), 184 Silicon Elastomer, and 184 Curing Agent, was purchased from SYLGARD. For 3D printer Vero Clear material and SUP706b supporting material were purchased from Stratasys. Hamilton gastight glass syringes (1000 series) which have volume of 1, 2.5, 10, and 25 mL, and were purchased from Hamilton. Polytetrafluoroethylene (PTFE) tubings (I.D. \times O.D. 0.5×1 mm; $1/16 \times 0.010$ inch) were purchased from Inacom.

Methods—Trypsin Activity Assay: The activity of trypsin was measured using a standard BAPNA assay by addition of trypsin solution to 0.7 mM BAPNA; 1.2% DMSO; 100 mM TRIS-HCl pH = 7.8 in MQ; 20 mM CaCl_2 ; RT ($\approx 22^\circ\text{C}$). The resulting absorbance was measured at 405 nm. Extinction coefficient for BAPNA measured was $6000 \text{ L mol}^{-1} \text{ cm}^{-1}$.

Methods—Continuous Flow Stirred Tank Reactor Experiments: A typical CFSTR experiment comprises two reactors *CFSTR1* and *CFSTR2*. *CFSTR1*

is fed by four separate inlets to supply Tg (1.04 mM in HCl, CaCl_2 4.20 mM), Tr (0.045 mM in HCl 4 mM), a buffer solution (TRIS-HCl, CaCl_2 , 100:20 mM, pH 7.8), and I (0.025 mM in buffer solution). The different reagents were flown in with fractions of the total flow rate (0.14, 0.08, 80–190, and 5–100, respectively), leading to initial concentrations in the reactor of Tg (0.156 mM), Tr (0.004 mM), I (0.005–0.010 mM) with 100 mM Tris-HCl, pH 7.7, 20 mM CaCl_2 as the final buffer solution in *CFSTR1* and a total flow rate of $250 \mu\text{M h}^{-1}$ (which in a 90 μL reactor results in $k_f = 3.3 \text{ h}^{-1}$).

CFSTR2 is fed by three separate inlets to supply BAPNA (4 mM in a mixture of MQ:DMFA:DMSO, 0.2:0.72:0.08), the outflow of *CFSTR1*, and a buffer solution. The different reagents were flown in with fractions of the total flow rate (0.25, 0.25, and 0.5, respectively), leading to initial concentrations in the reactor of BAPNA (1.0 mM) and Tr (varied depending on the process), with the mixture (Tris-HCl, pH 7.7, 20 mM

CaCl₂:(DMFA:DMSO) as the final buffer solution in CFSTR2 and a total flow rate of 1000 μM h⁻¹ (which in a 80 μL reactor results in $k_f = 12.5 \text{ h}^{-1}$ ensuring fast online detection). See Section S3, Supporting Information, for details on the fabrication of poly(dimethylsiloxane) (PDMS) reactors, calibration of the detection unit, and syringe pumps settings.

Methods—Mathematical Modelling: For phase plot simulations, $\Delta[Tr]$ was calculated using a protocol comprising two steps: For each grid, $[Tr]$ (t) was simulated using a numerical solver from two different starting points (i.e., from a high $[Tr]_{ss}$ and low $[Tr]_{ss}$). Second, the steady states were established that were preceded by a high $[Tr]_{ss}$ (i.e., when $[I]_{-1} = 0.5$) from those that were preceded by a low $[Tr]_{ss}$ (i.e., when $[I]_{-1} = 10$). A subtraction resulted in $\Delta[Tr]$ reported in Figure 2d, with the borders of used parameter spaces defined in the figure.

For LIS simulations, time series were simulated with a programmed input inhibitor concentration sequence comprising a negative gradient that switches from $[I]_{-1}$ to $[I]_0$, and a positive gradient to returns to $[I]_0$. The derivative was determined in each individual step of the sequence (60 data points per sweep).

The methods use a previously reported mathematical model based on mass action kinetics, summarized in Section S4.1, Supporting Information.^[20] The scripts are provided as part of the online Supporting Information. For further details, and explanation of the working scripts, see Sections S4.2–S4.3, Supporting Information.

Supporting Information

Supporting Information is available from the Wiley Online Library or from the author.

Acknowledgements

The work was supported by the Netherlands Organization for Scientific Research (NWO, Veni Grant 202.155 (A.S.Y.W.)).

Conflict of Interest

The authors declare no conflict of interest.

Data Availability Statement

The data that support the findings of this study are available in the supplementary material of this article.

Keywords

adaptation, autocatalysis, bistability, chemical reaction networks, hysteresis, molecular computing

Received: December 4, 2021

Revised: February 2, 2022

Published online: March 8, 2022

[1] V. Sze, Y.-H. Chen, T.-J. Yang, J. S. Emer, *Proc. IEEE* **2017**, *105*, 2295.

[2] N. Jones, *Nature* **2018**, *561*, 163.

[3] C. Kaspar, B. J. Ravoo, W. G. van der Wiel, S. V. Wegner, W. H. P. Pernice, *Nature* **2021**, *594*, 345.

[4] L. Qian, E. Winfree, J. Bruck, *Nature* **2011**, *475*, 368.

[5] K. M. Cherry, L. Qian, *Nature* **2018**, *559*, 370.

- [6] J. M. Parrilla-Gutierrez, A. Sharma, S. Tsuda, G. J. T. Cooper, G. Aragon-Camarasa, K. Donkers, L. Cronin, *Nat. Commun.* **2020**, *11*, 1442.
- [7] S. Goswami, R. Pramanick, A. Patra, S. P. Rath, M. Foltin, A. Ariando, D. Thompson, T. Venkatesan, S. Goswami, R. S. Williams, *Nature* **2021**, *597*, 51.
- [8] C. P. Collier, E. W. Wong, M. Belohradský, F. M. Raymo, J. F. Stoddart, P. J. Kuekes, R. S. Williams, J. R. Heath, *Science* **1999**, *285*, 391.
- [9] A. J. Ruben, L. F. Landweber, *Nat. Rev. Mol. Cell Biol.* **2000**, *1*, 69.
- [10] A. Adamatzky, B. D. L. Costello, T. Shirakawa, *Int. J. Bifurcation Chaos* **2008**, *18*, 2373.
- [11] P. Sundberg, M. Karppinen, *Beilstein J. Nanotechnol.* **2014**, *5*, 1104.
- [12] B. Novák, J. J. Tyson, *Nat. Rev. Mol. Cell Biol.* **2008**, *9*, 981.
- [13] J. J. Tyson, K. C. Chen, B. Novák, *Curr. Opin. Cell Biol.* **2003**, *15*, 221.
- [14] A.-L. Barabási, Z. N. Oltvai, *Nat. Rev. Genet.* **2004**, *5*, 101.
- [15] R. Milo, S. Shen-Orr, S. Itzkovitz, N. Kashtan, D. Chklovskii, U. Alon, *Science* **2002**, *298*, 824.
- [16] J. H. van Esch, R. Klajn, S. Otto, *Chem. Soc. Rev.* **2017**, *46*, 5474.
- [17] M. Feinberg, *Foundations of Chemical Reaction Network Theory*, Springer, New York **2019**.
- [18] G. Craciun, M. Feinberg, *SIAM J. Appl. Math.* **2006**, *66*, 1321.
- [19] G. Shinar, M. Feinberg, *Science* **2010**, *327*, 1389.
- [20] S. N. Semenov, L. J. Kraft, A. Ainla, M. Zhao, M. Baghbanzadeh, V. E. Campbell, K. Kang, J. M. Fox, G. M. Whitesides, *Nature* **2016**, *537*, 656.
- [21] S. N. Semenov, A. S. Y. Wong, R. M. van der Made, S. G. J. Postma, J. Groen, H. W. H. van Roekel, T. F. A. de Greef, W. T. S. Huck, *Nat. Chem.* **2015**, *7*, 160.
- [22] J. Boekhoven, W. E. Hendriksen, G. J. M. Koper, R. Eelkema, J. H. van Esch, *Science* **2015**, *349*, 1075.
- [23] J. M. A. Carnall, C. A. Waudby, A. M. Belenguer, M. C. A. Stuart, J. J.-P. Peyralans, S. Otto, *Science* **2010**, *327*, 1502.
- [24] R. Merindol, A. Walther, *Chem. Soc. Rev.* **2017**, *46*, 5588.
- [25] L. O. Chua, S. M. Kang, *Proc. IEEE* **1976**, *64*, 209.
- [26] J. Tang, F. Yuan, X. Shen, Z. Wang, M. Rao, Y. He, Y. Sun, X. Li, W. Zhang, Y. Li, B. Gao, H. Qian, G. Bi, S. Song, J. J. Yang, H. Wu, *Adv. Mater.* **2019**, *31*, 1902761.
- [27] S. G. J. Postma, D. te Brinke, I. N. Vialshin, A. S. Y. Wong, W. T. S. Huck, *Tetrahedron* **2017**, *73*, 4896.
- [28] J. E. Ferrell, S. H. Ha, *Trends Biochem. Sci.* **2014**, *39*, 612.
- [29] I. R. Epstein, K. Showalter, *J. Phys. Chem.* **1996**, *100*, 13132.
- [30] D. Bray, *Nature* **1995**, *376*, 307.
- [31] B. N. Kholodenko, *Nat. Rev. Mol. Cell Biol.* **2006**, *7*, 165.
- [32] J. E. Purvis, G. Lahav, *Cell* **2013**, *152*, 945.
- [33] J. Zhou, C. Liu, C. Tsou, *Biochemistry* **1989**, *28*, 1070.
- [34] A. Sawa, *Mater. Today* **2008**, *11*, 28.
- [35] L. Gammaitoni, P. Hänggi, P. Jung, F. Marchesoni, *Rev. Mod. Phys.* **1998**, *70*, 223.
- [36] N. Perunov, R. A. Marsland, J. L. England, *Phys. Rev. X* **2016**, *6*, 021036.
- [37] B. A. Grzybowski, W. T. S. Huck, *Nat. Nanotechnol.* **2016**, *11*, 585.
- [38] J.-C. Galas, A.-M. Haghiri-Gosnet, A. A. Estévez-Torres, *Lab Chip* **2012**, *13*, 415.
- [39] G. Gines, A. S. Zadorin, J.-C. Galas, T. Fujii, A. Estevez-Torres, Y. Rondelez, *Nat. Nanotechnol.* **2017**, *12*, 351.
- [40] A. E. Zoheir, G. P. Späth, C. M. Niemeyer, K. S. Rabe, *Small* **2021**, *17*, 2007166.
- [41] A. A. Pogodaev, C. L. F. Regueiro, M. Jakštaitė, M. J. Hollander, W. T. S. Huck, *Angew. Chem.* **2019**, *58*, 14539.
- [42] C. E. Arcadia, A. Dombroski, K. Oakley, S. L. Chen, H. Tann, C. Rose, E. Kim, S. Reda, B. M. Rubenstein, J. K. Rosenstein, *Chem. Sci.* **2021**, *12*, 5464.
- [43] A. Blokhuis, D. Lacoste, P. Nghe, *Proc. Natl. Acad. Sci. U.S.A.* **2020**, *117*, 25230.